PAPER

Physics of plasma burn-through and DYON simulations for the JET ITER-like wall

IOP Publishing and International Atomic Energy Agency Nuclear Fusion
Nucl. Fusion **53** (2013) 083024 (16pp) doi:10.1088/0029-5515/53/8/083024

Physics of plasma burn-through and DYON simulations for the JET ITER-like wall

Hyun-Tae Kim[1,2], **A.C.C. Sips**[1,3] **and EFDA-JET Contributors**[a]

JET-EFDA Culham Science Centre, Abingdon, OX14 3DB, UK
[1] Department of Physics, Imperial College London, Prince Consort Road, London, SW7 2AZ, UK
[2] EURATOM/CCFE Fusion Association, Abingdon, OX14 3DB, UK
[3] JET/EFDA, Culham Science Centre, Abingdon, OX14 3DB, UK

E-mail: hyun.kim09@imperial.ac.uk

Received 14 December 2012, accepted for publication 10 June 2013
Published 24 July 2013
Online at stacks.iop.org/NF/53/083024

Abstract
This paper presents the DYON simulations of the plasma burn-through phase at Joint European Torus (JET) with the ITER-like wall. The main purpose of the study is to validate the simulations with the International Thermonuclear Experimental Reactor (ITER)-like wall, made of beryllium. Without impurities, the burn-through process of a pure deuterium plasma is described using DYON simulations, and the criterion for deuterium burn-through is derived analytically. The plasma burn-through with impurities are simulated using wall-sputtering models in the DYON code, which are modified for the ITER-like wall. The wall-sputtering models and the validation against JET data are presented. The impact of the assumed plasma parameters in DYON simulations are discussed by means of parameter scans. As a result, the operation space of prefill gas pressure and toroidal electric field for plasma burn-through in JET is compared with the Townsend avalanche criterion.

(Some figures may appear in colour only in the online journal)

1. Introduction

1.1. Motivation

Tokamak start-up consists of the electron avalanche phase, the plasma burn-through phase and the ramp-up phase of the plasma current I_p [2]. The Townsend avalanche theory [3, 4] is generally used to calculate the required electric field for electron avalanche ($E_{\text{avalanche}}$) at a given prefill gas pressure p and effective connection length L_f as shown below:

$$E_{\text{avalanche}}(\text{V m}^{-1}) \geqslant \frac{1.25 \times 10^4 \times p(\text{Torr})}{\ln(510 \times p(\text{Torr}) \times L_f(\text{m}))}. \quad (1.1)$$

The required $E_{\text{avalanche}}$ for plasma initiation in the International Thermonuclear Experimental Reactor (ITER) has also been calculated using equation (1.1) as presented in the ITER Physics Basis [2].

However, the Townsend avalanche theory is not sufficient to explain all non-sustained break-down discharges. In order for plasma current to increase, sufficient ionization of the prefill gas (deuterium) and impurities, i.e. plasma burn-through, is necessary. Otherwise, most heating power is lost through radiation and ionizations of the remaining neutrals, so that it prevents electron temperature from increasing in the ramp-up phase of plasma current [3]. It should be noted that the required loop voltage for plasma burn-through, the burn-through criterion, is generally higher than that for electron avalanche in present tokamaks [2], and a number of start-up failures in current devices result from the failure of plasma burn-through. For experiments with the carbon wall in Joint European Torus (JET), more than 85% of all non-sustained break-down failures occurred during the plasma burn-through phase [5]. These start-up failures could be reduced by understanding key physics aspects of the plasma burn-through phase.

Furthermore, due to the engineering issues in ITER, resulting from the use of superconducting central solenoid coils and a continuous vacuum vessel, the maximum toroidal electric field on-axis is limited up to 0.35 V m^{-1} [6], which is much lower than the typical toroidal electric field used for plasma burn-through in current devices, e.g. $\sim$1 V m^{-1} in JET. Tokamak start-up using such a low electric field limits the operation space available for the range of prefill gas pressure, magnetic error fields, and impurity content [7]. In order to

[a] See the appendix of [1].

obtain more confidence in the start-up scenario at ITER, a predictive simulation for plasma burn-through is required.

For reliable start-up using a low electric field, RF-assisted start-up using electron cyclotron heating (ECH) [8] or ion cyclotron heating (ICH) [9] is planned in ITER. However, launching excessive RF power into the vacuum vessel without a plasma or with a very low temperature plasma can result in serious damage to the diagnostic systems, due to the low absorption efficiency of the RF power. Hence, in order to estimate the required ECH power (although not presented in this paper) understanding the plasma burn-through conditions (or requirements) is also important.

The DYON (DYnamic 0D model of Non-fully ionized plasma) code is a plasma burn-through simulator, developed at JET. In the DYON code, the confinement time is modelled as a function of plasma parameters considering parallel transport as well as perpendicular transport, and the impurity influx is calculated using wall-sputtering models. The impurity densities in each charge state are calculated self-consistently by particle balances in non-coronal equilibrium. In this calculation, neutral screening effects are also taken into account, and the atomic reactions and the resultant radiation are computed using the Atomic Data and Analysis Structure (ADAS) package [10]. A detailed description of the DYON code can be found in [11].

The DYON simulation results show a reasonable agreement with JET data with the carbon wall [11]. The recent installation of the ITER-like wall at JET i.e. a combination of beryllium and tungsten protection tiles [12], enabled us to validate the wall-sputtering models for a beryllium wall with results from recent experiments. In this paper, the modified wall-sputtering model in the DYON code will be explained, and the simulation results are compared with JET data with the ITER-like wall. Using the validated models, the operation window of prefill gas pressure and toroidal electric field for plasma burn-through in JET is computed, and it is compared with the Townsend criterion.

1.2. Structure of the paper

Plasma burn-through of a pure deuterium plasma will be discussed in section 2. In section 3, the previous wall-sputtering model for the carbon wall is reviewed. In section 4, the modification of the wall-sputtering model for the JET ITER-like wall will be introduced. In section 5, DYON simulation results for the JET ITER-like wall are compared with JET data to provide a validation. The effects of the parameters assumed in the DYON simulation, i.e. deuterium recycling coefficient, fuelling efficiency and initial carbon content, will be investigated in section 5. In section 6, the computed criterion for plasma burn-through with impurities is compared with the Townsend avalanche criterion, and the operation space for JET is presented. Discussion and conclusions are given in sections 7 and 8, respectively.

2. Physics of deuterium burn-through

Impurities during the plasma burn-through phase result from complex plasma surface interaction. This makes analytical investigation on plasma burn-through extremely complicated.

Table 1. Plasma parameters assumed for DYON simulations (figures 1, 2, 4, 5 and 13).

Plasma parameters	Input values
Toroidal magnetic field B_ϕ	2.3 T
Vertical magnetic field B_v	0.001 T
Initial plasma current density $J_\mathrm{p}(0)$	$382.5 \times E = 405.8\,\mathrm{A\,m^{-2}}$
Initial eddy current $I_{\mathrm{MK2}}(0)$	0 A
Initial electron temperature $T_\mathrm{e}(0)$	1 eV
Initial ion temperature $T_\mathrm{i}(0)$	0.03 eV
Prefilled gas pressure $p(0)$	Figures 1 and 2 : 5 and $7(\times 10^{-5}$ Torr)
	Figure 4 : 1, 3, 5 and $7(\times 10^{-5}$ Torr)
	Figure 5 : 5×10^{-5} Torr
	Figure 13 : 1×10^{-6}–2×10^{-4} Torr
Initial D atom density $n^0_\mathrm{D}(0)$	$2.78 \times 10^{22} \times p(0)$ Torr
Initial degree of ionization $\gamma_\mathrm{iz}(0)$	0.002
Initial impurity $n^0_\mathrm{I}(0)$	0
Y^D_D	1
Fuelling efficiency	0% i.e. No additional fuelling
PSI model	Figures 1, 2 and 4 : no PSI effects
	Figures 5 and 13 : no PSI, C wall or Be wall
Plasma major radius R	3 m
Plasma minor radius a	Figures 1, 2 and 4 : 0.5 m
	Figures 5 and 13 : 0.9 m
Internal inductance l_i	0.5
Loop voltage U_l	20 V
Effective vessel volume	$100\,\mathrm{m^{-3}}$

To gain an insight into the key physics aspects in the plasma burn-through phase, it is worth starting the investigation of a pure deuterium plasma. Furthermore, according to recent observation in JET with the ITER-like wall, deuterium radiation can be critical for plasma burn-through with a beryllium wall.

The results presented in this section are obtained by DYON simulations (figures 1, 2 and 4) without any impurity model. Figure 3 is drawn using an analytical formula. The plasma parameters assumed in the DYON simulations of a pure deuterium plasma are given in table 1. In order to simulate the cases of successful and failed plasma burn-through, two different prefill gas pressures are assumed, 5×10^{-5} Torr (success) and 7×10^{-5} Torr (failure) in figures 1 and 2[4]. In figure 4, a wider range of prefill gas pressures (1×10^{-5}, 3×10^{-5}, 5×10^{-5} and 7×10^{-5} Torr) is used to show the effects of prefill gas pressure on plasma burn-through.

2.1. Condition for plasma current ramp-up

Assuming no eddy current in the passive structure, the plasma current I_p in tokamaks can be calculated with the circuit equation

$$I_\mathrm{p} = \frac{1}{R_\mathrm{p}}\left(U_\mathrm{l} - L_\mathrm{p}\frac{\mathrm{d}I_\mathrm{p}}{\mathrm{d}t}\right), \tag{2.1}$$

where R_p, U_l and L_p are plasma resistance, loop voltage and plasma inductance, respectively. In order for I_p to increase for

[4] 1 Torr = 1.333 223 68 mbar.

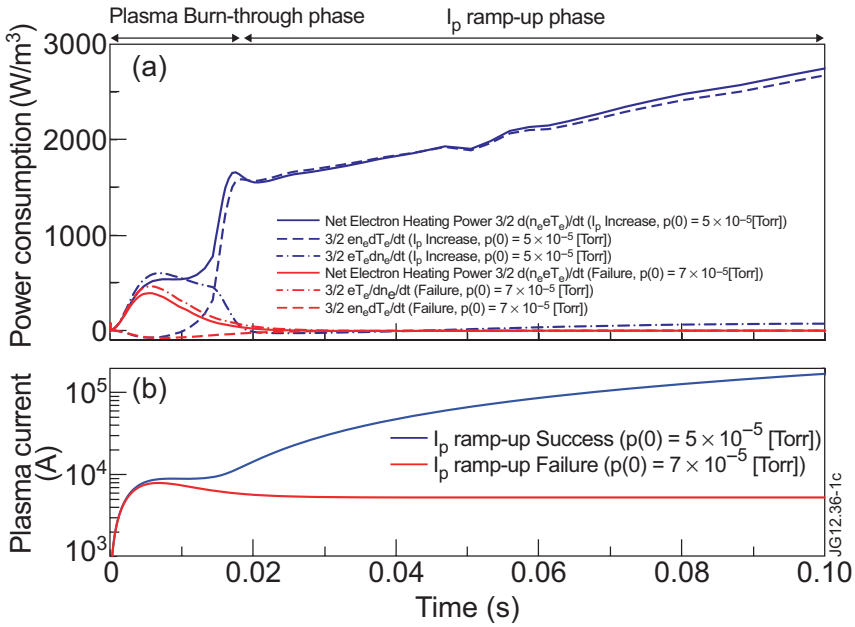

Figure 1. DYON simulation results for a pure deuterium plasma. The colours of lines in (*a*) and (*b*) indicate successful I_p ramp-up (blue) and failure (red). The solid lines represent the net electron heating power P_e. The dashed lines and the chain lines are the amount of P_e consumed by increasing T_e and increasing n_e, respectively. The corresponding plasma currents I_p are represented by the blue solid line (I_p ramp-up) and the red solid line (non-sustained break-down) in (*b*). In order for I_p to increase, P_e must be positive in the I_p ramp-up phase.

a given U_l, which is approximately constant in the I_p ramp-up phase, R_p must be decreasing continuously. According to Spitzer resistivity, R_p decreases as T_e increases [13], i.e. $R_p \propto T_e^{-\frac{3}{2}}$. Therefore,

$$\frac{dT_e}{dt} > 0 \tag{2.2}$$

is a necessary condition for I_p ramp-up.

Whether or not T_e increases is determined by the equation for electron energy balance,

$$P_e = \frac{3}{2}\frac{d(n_e k T_e)}{dt} = \frac{3}{2}kT_e\frac{dn_e}{dt} + \frac{3}{2}n_e\frac{dkT_e}{dt}, \tag{2.3}$$

where P_e is the net electron heating power, determined by the ohmic heating power P_{Oh} (for cases without the assistance of additional heating) and the total electron power loss P_{Loss}, i.e. $P_e = P_{Oh} - P_{Loss}$. As separated into the two terms in equation (2.3), the net electron heating power P_e is consumed by increasing n_e or T_e, i.e. $\frac{3}{2}kT_e\frac{dn_e}{dt}$ or $\frac{3}{2}n_e\frac{dkT_e}{dt}$.

The change of equation (2.3) during the plasma burn-through phase is described in figure 1 using the DYON simulation results: (*a*) the power consumption for successful I_p ramp-up (blue) and the failed case (red) and (*b*) the corresponding plasma current in each case. As shown, P_e is positive for the successful case, and goes to zero in the failed case during the I_p ramp-up phase. Whereas the power consumed by the increasing n_e (chain lines) is dominant in the plasma burn-through phase, it is small enough to be ignored in the I_p ramp-up phase as shown in figure 1(*a*), i.e. blue solid line ≈ blue dashed line. Therefore, P_e in the I_p ramp-up phase can be approximated to be $P_e \approx \frac{3}{2}n_e\frac{dkT_e}{dt}$. Accordingly, in order for T_e to increase, P_e must be positive in the I_p ramp-up phase, i.e.

$$P_e > 0. \tag{2.4}$$

In this simulation, the deuterium recycling coefficient Y_D^D is assumed as 1. In the case that Y_D^D is higher than 1, the power consumed by the increasing n_e would not be 0. However, equation (2.4) is still a necessary condition for the increase in T_e unless the power consumed by the increasing n_e becomes significant.

Figure 2 shows DYON simulation results for P_{Oh} and P_{Loss} in the case of I_p ramp-up success (blue) and failure (red), respectively. In the successful case, P_{Oh} (blue solid line) exceeds P_{Loss} (blue dashed line), i.e. positive P_e in the I_p ramp-up phase. However, P_{Oh} (red solid line) and P_{Loss} (red dashed line) overlap in the failed case, hence P_e is zero. Figure 2(*b*), which is enlarged from figure 2(*a*), shows that the behaviour of P_e in the burn-through phase are clearly different in the two cases. It is determined by the behaviour of P_e during the plasma burn-through phase whether P_e in the I_p ramp-up phase is positive. Hence, P_e during the plasma burn-through phase should be investigated to derive the requirement of I_p ramp-up, i.e. the criterion of plasma burn-through.

2.2. *Criterion for deuterium burn-through*

The total electron power loss, P_{Loss}, consists of the three power loss terms, i.e. radiation and ionization power loss P_{rad+iz}, equilibration power loss P_{equi} and convective transport power loss P_{conv}^e. In the case of a pure deuterium plasma assumed in this section, they are calculated as shown below [7, 11].

$$P_{Loss} = P_{rad+iz} + P_{equi} + P_{conv}^e$$
$$P_{rad+iz} = V_p \times \mathcal{P}_{RI}(T_e) n_e n_D^0 \tag{2.5}$$

$$P_{equi} = V_p \times 7.75 \times 10^{-34}(T_e - T_i)\frac{n_e n_D^{1+} \ln\Lambda}{T_e^{3/2} M_D} \tag{2.6}$$

$$P_{conv}^e = V_p \times \frac{3}{2}\frac{n_e k T_e}{\tau_e}, \tag{2.7}$$

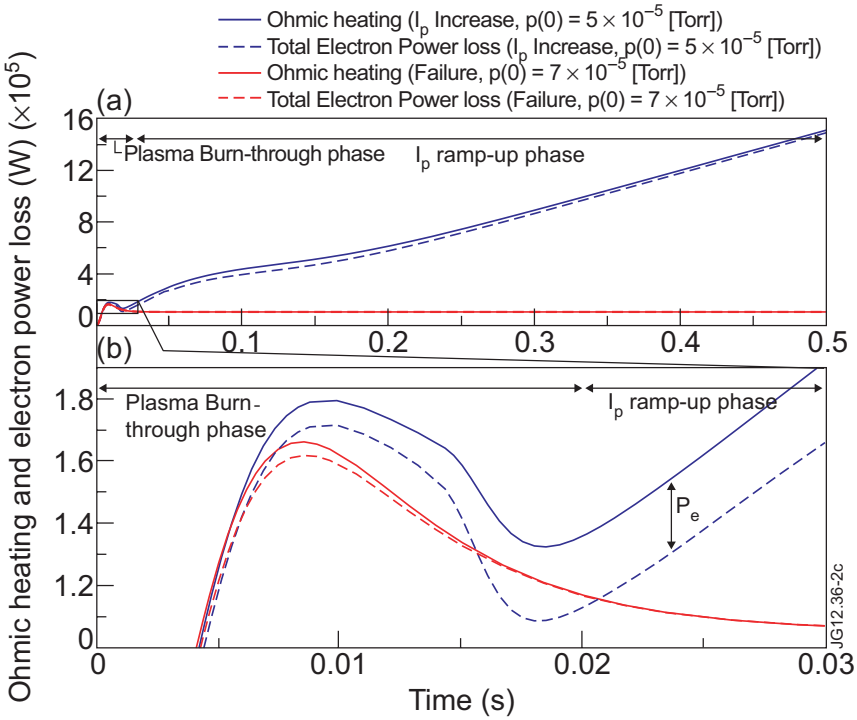

Figure 2. DYON simulation results for a pure deuterium plasma. The solid lines and the dashed lines in (*a*) show $P_{\rm Oh}$ and $P_{\rm Loss}$ in successful (blue) and failure (red) cases, respectively. (*b*) is an expanded figure from the burn-through phase in (*a*). It is determined by $P_{\rm e}$ during the plasma burn-through phase whether $P_{\rm e}$ is positive for the $I_{\rm p}$ ramp-up phase.

where $n_{\rm D}^0$ is the deuterium atom density, $n_{\rm D}^{1+}$ is the deuterium ion density, $V_{\rm p}$ is the plasma volume, $M_{\rm D}$ is the deuterium ion mass in amu, $\tau_{\rm e}$ is the electron particle confinement time, and $\mathcal{P}_{\rm RI}(T_{\rm e})$ is the power loss coefficient due to the radiation and ionization, obtained from ADAS package [10].

In contrast to $P_{\rm equi}$ and $P_{\rm conv}^{\rm e}$, which simply increase with $n_{\rm e}$, $P_{\rm rad+iz}$ has a maximum value at a certain degree of ionization since $n_{\rm D}^0$ decreases as $n_{\rm e}$ increases. In this paper, we define the peak value of $P_{\rm rad+iz}$ as the *radiation and ionization barrier* (RIB), and the degree of ionization at the RIB is defined to be the *critical degree of ionization* for plasma burn-through, $\gamma_{\rm iz}(t_{\rm RIB})$.

The RIB is of crucial importance since the required $P_{\rm Oh}$ for $I_{\rm p}$ ramp-up is mainly determined by the RIB. As will be shown, the magnitude of $P_{\rm rad+iz}$ is dominant in $P_{\rm Loss}$ during the plasma burn-through phase. This implies that $P_{\rm Loss}$ also has the maximum value at $\gamma_{\rm iz}(t_{\rm RIB})$. Hence, once the $P_{\rm Oh}$ exceeds the $P_{\rm Loss}$ maximum, $P_{\rm Loss}$ decreases significantly as ionizations proceed. This enables $T_{\rm e}$ to increase, so that ionizations continue to increase up to 100%, i.e. full ionization.

During the plasma burn-through phase, the density of deuterium atoms $n_{\rm D}^0(t)$ decreases, thereby increasing $n_{\rm e}(t)$. When the deuterium atom density within a plasma volume decreases, neutral particles flow into the plasma volume from the ex-plasma volume, giving a dynamic fuelling effect. This effect maintains a neutral density within a plasma volume as much as the ratio of plasma volume to total neutral volume (= effective vessel volume $V_{\rm V}$, in which all neutrals are accessible to the plasma). The effective reduction in neutral density in $V_{\rm p}$ is $\frac{V_{\rm p}}{V_{\rm V}}n_{\rm e}(t)$. Hence, in the case that the deuterium recycling coefficient $Y_{\rm D}^D$ is 1 and there is no gas pumping or puffing, $n_{\rm D}^0$ in equation (2.5) is

$$n_{\rm D}^0(t) = n_{\rm D}^0(0) - \frac{V_{\rm p}}{V_{\rm V}}n_{\rm e}(t), \tag{2.8}$$

where $n_{\rm D}^0(0)$ indicates the initial density of deuterium atoms, which is proportional to the prefill gas pressure. By substituting $n_{\rm D}^0$ in equation (2.5) with $n_{\rm D}^0(t)$ in equation (2.8), $P_{\rm rad+iz}(t)$ can be written as a quadratic function of $n_{\rm e}(t)$,

$$\begin{aligned} P_{\rm rad+iz}(t) &= V_{\rm p}\mathcal{P}_{\rm RI}(T_{\rm e})n_{\rm e}(t)n_{\rm D}^0(t) \\ &= V_{\rm p}\mathcal{P}_{\rm RI}(T_{\rm e})n_{\rm e}(t)\left(n_{\rm D}^0(0) - \frac{V_{\rm p}}{V_{\rm V}}n_{\rm e}(t)\right) \\ &= V_{\rm p}\mathcal{P}_{\rm RI}(T_{\rm e})\left(\frac{V_{\rm V}n_{\rm D}^0(0)^2}{4V_{\rm p}} - \frac{V_{\rm p}}{V_{\rm V}}\left(n_{\rm e}(t) - \frac{V_{\rm V}n_{\rm D}^0(0)}{2V_{\rm p}}\right)^2\right). \end{aligned} \tag{2.9}$$

Therefore, as ionizations proceed, $n_{\rm e}(t)n_{\rm D}^0(t)$ in equation (2.9) has a maximum value. Figure 3(*a*) indicates the change in $n_{\rm e}(t)n_{\rm D}^0(t)$ with the normalized $n_{\rm e}(t)$, i.e. $\frac{n_{\rm e}(t)V_{\rm p}}{n_{\rm D}^0(0)V_{\rm V}}$. As shown in figure 3(*a*), $n_{\rm e}(t)n_{\rm D}^0(t)$ has the maximum value

$$\frac{V_{\rm V}n_{\rm D}^0(0)^2}{4V_{\rm p}}, \tag{2.10}$$

when $n_{\rm e}(t)$ is equal to

$$\frac{V_{\rm V}n_{\rm D}^0(0)}{2V_{\rm p}}. \tag{2.11}$$

The power coefficient $\mathcal{P}_{\rm RI}(T_{\rm e})$ is a function of $T_{\rm e}$. Figure 3(*b*) shows $\mathcal{P}_{\rm RI}(T_{\rm e})$ obtained from the ADAS package [10]. The

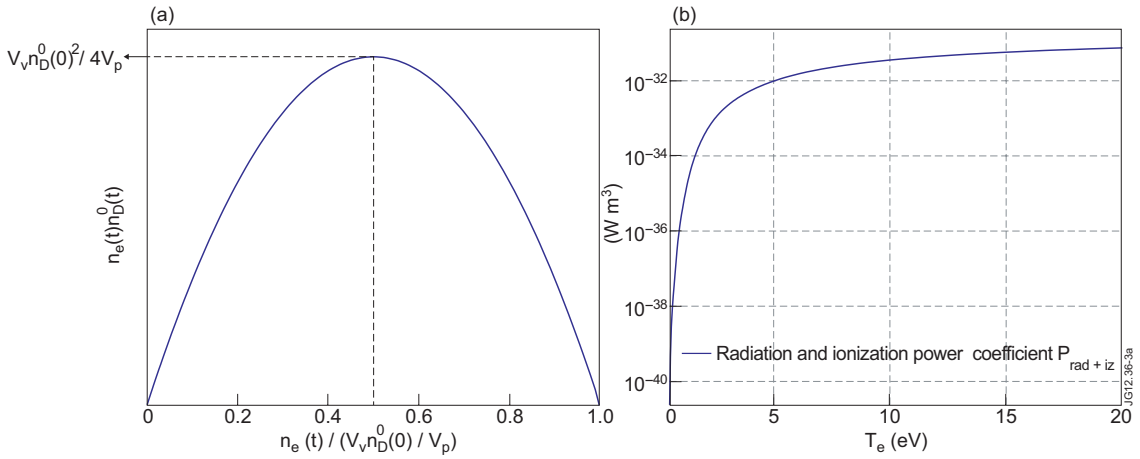

Figure 3. (*a*) shows the change in $n_e(t)n_D^0(t)$ with the normalized n_e. Since $n_e(t)n_D^0(t)$ can be substituted by $n_e(t)(n_D^0(0) - n_e(t))$ in the case of a recycling coefficient (= 1.0), it has a maximum value as $n_e(t)$ approaches equation (2.11). (*b*) indicates the electron power loss coefficient due to the radiation and ionization of deuterium, $\mathcal{P}_{RI}$, obtained from ADAS. $\mathcal{P}_{RI}$ is strongly dependent on T_e only.

product of $n_e(t)n_D^0(t)$ and $\mathcal{P}_{RI}(T_e)$ results in the change of P_{rad+iz}, thereby the change of P_{Loss} in figure 2.

The degree of ionization in the plasma burn-through phase can be calculated with

$$\gamma_{iz}(t) = \frac{n_e(t)}{n_e(t) + n_D^0(t)}. \tag{2.12}$$

The degree of ionization at the RIB, $\gamma_{iz}(t_{RIB})$, is then obtained by substituting $n_D^0(t)$ and $n_e(t)$ with equations (2.8) and (2.11) as shown below:

$$\begin{aligned}\gamma_{iz}(t_{RIB}) &= \frac{\frac{V_v n_d^0(0)}{2V_p}}{\frac{V_V n_d^0(0)}{2V_p} + \left(n_D^0(0) - \frac{V_p \frac{V_v n_d^0(0)}{2V_p}}{V_V}\right)} \\ &= \frac{V_V}{V_V + V_p}.\end{aligned} \tag{2.13}$$

The plasma volume is limited by the vessel volume, i.e. $V_p \leqslant V_V$. This implies that $\gamma_{iz}(t_{RIB})$ is always higher than 50%. In the case of JET, where V_V is $\sim$100 m^3 (further explanation on V_V is provided in section 7) and initial plasma volume $V_p = 14.8$–59.2 m^3 (major radius $R = 3$ m and minor radius $a = 0.5$–1 m), the critical degree of ionization $\gamma_{iz}(t_{RIB})$ is 87.1–62.8%, respectively.

Figure 4 shows DYON simulation results of (*a*) plasma current, (*b*) degree of ionization and (*c*) electron power losses for different prefill gas pressures. The I_p ramp-up is delayed until almost 100% ionization is achieved in the low prefill gas pressure cases (1×10^{-5}, 3×10^{-5} and 5×10^{-5} Torr), and the delay is extended with increasing prefill gas pressures. The I_p ramp-up fails at a prefill gas pressure over 7×10^{-5} Torr. This indicates that above a prefill gas pressure of 7×10^{-5} Torr the given loop voltage is not sufficient to achieve the critical degree of ionization, $\gamma_{iz}(t_{RIB})$, as shown in figure 4(*b*). That is, the maximum prefill gas pressure available for plasma burn-through with the given 20 V loop voltage exists between 5×10^{-5} and 7×10^{-5} Torr.

For the low prefill gas pressure cases, the corresponding peak values of P_{rad+iz} in figure 4(*c*) indicate the RIB. As shown in figure 4(*c*), P_{iz+rad} is dominant in P_{Loss} during the plasma burn-through phase, and the peak of P_{Loss} coincides with the RIBs. Therefore, the required electric field for plasma burn-through is mainly determined by P_{iz+rad}. It should be noted that the RIB rises as prefill gas pressure increases in figure 4(*c*). This is due to the fact that neutrals are strong energy sinks. That is, the larger number of neutrals at a high prefill gas pressure results in higher P_{rad}. In addition, there are more neutrals to be ionized at a high prefill gas pressure, thereby increasing P_{iz}.

The increase in RIB can also be seen in equation (2.9). Equation (2.9) indicates that the maximum $P_{rad+iz}(t_{RIB})$ is

$$P_{rad+iz}(t_{RIB}) = \frac{V_V \mathcal{P}_{RI}(T_e) n_D^0(0)^2}{4}. \tag{2.14}$$

$n_D^0(0)$ is proportional to the prefill gas pressure p. Hence, $P_{rad+iz}(t_{RIB})$ also increases proportionally with the square of p, if T_e is identical at the t_{RIB}. Since T_e during the plasma burn-through phase does not vary significantly, equation (2.14) is another indication for the increase in RIB with prefill gas pressure.

The required electric field to overcome the RIB, E_{RIB}, can also be calculated using equation (2.14), i.e. $P_{Oh} = P_{rad+iz}(t_{RIB})$. Since the ohmic heating power P_{Oh} is $V_p(E^2/\eta_s)$, the required electric field E_{RIB} is

$$\begin{aligned}E_{RIB}^2 &= \frac{\eta_s V_V \mathcal{P}_{RI}(T_e) n_D^0(0)^2}{4V_p} \\ E_{RIB} &= 0.011 \sqrt{\frac{V_V \mathcal{P}_{RI}(T_e)}{V_p T_e^{3/2}}} \times n_D^0(0),\end{aligned} \tag{2.15}$$

where η_s is Spitzer resistivity, i.e. $\eta_s = 5 \times 10^{-4} \times T_e^{-3/2}$ eV [13].

3. Review of wall-sputtering models for a carbon wall

In the previous section, the burn-through process of a pure deuterium plasma was described. Now, impurity effects are taken into account.

In the carbon wall, chemical sputtering, emitting hydrocarbon molecules such as CD_4, is dominant if T_e is

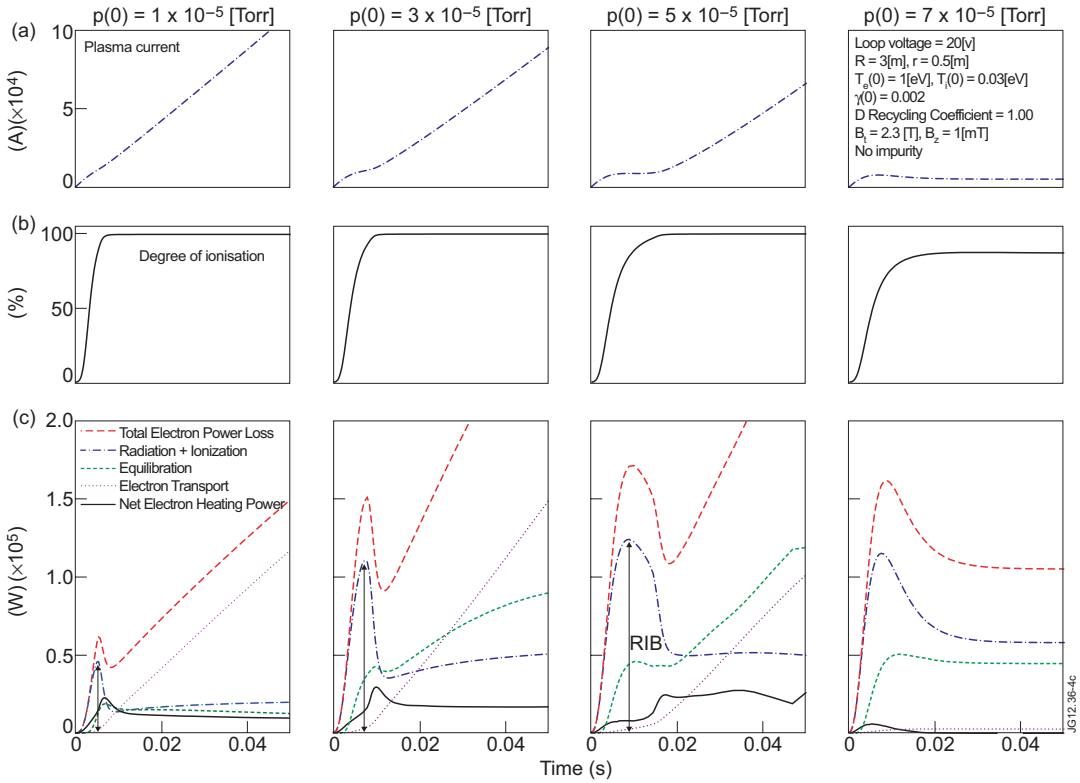

Figure 4. DYON simulation results for a pure deuterium plasma. The figures show (*a*) the plasma current, (*b*) the degree of ionization and (*c*) various electron power losses at different prefill gas pressures, 1×10^{-5}, 3×10^{-5}, 5×10^{-5} and 7×10^{-5} Torr. The assumed loop voltage and plasma parameters are shown in table 1. Under the given condition, a critical prefill gas pressure for I_p ramp-up exists between 5×10^{-5} and 7×10^{-5} Torr. Prefill gases are almost fully ionized in the cases of successful I_p ramp-up while they are not fully ionized in the cases of failure. The coloured lines in (*c*) indicate P_{Loss} (dashed red), P_{equi} (dashed green), $P^{\mathrm{e}}_{\mathrm{conv}}$ (dotted cyan) and $P_{\mathrm{rad+iz}}$ (chain blue), respectively. As shown in (*c*), $P_{\mathrm{rad+iz}}$ is dominant in P_{Loss} during the burn-through phase, and its peak values coincide the RIB. The RIB increases with prefill gas pressure, thereby increasing P_{Loss} maximum. That is, the higher the prefill gas pressure, the larger the P_{Loss} maximum.

lower than 100 eV, which is the case for the plasma burn-through phase. Since the chemical sputtering yield is weakly dependent on the incident ion energy, the carbon sputtering yield due to deuterium ion bombardment is assumed to be a constant 0.03, based on the experimental data from laboratory plasmas [14]. In the case of oxygen ion bombardment, most oxygen ions are recycled as carbon monoxide, CO, at a carbon target [15]. According to this, oxygen sputtering is also modelled for the carbon-wall JET with a constant sputtering yield, 1. The details of the chemical sputtering model used are given in [11]. The DYON simulation results using the wall-sputtering model for the carbon wall have shown good agreement with the experimental data of JET with the carbon wall as presented in [11]. However, it should be noted that the chemical sputtering model used was a simplified model, without considering some issues such as chemical sputtering by neutrals, physical sputtering and a-CH film formation on the wall surface. These can increase the carbon sputtering yield.

One of the important features with the carbon wall is that the electron power loss is dominated by the carbon burn-through. Figure 5 shows DYON simulation results of the electron power losses due to radiation and ionization with different wall models at JET: with a carbon wall (dotted blue), with a beryllium wall (dashed red), or for a pure deuterium plasma (solid black). In the case of the carbon wall in figure 5, the second peak of $P_{\mathrm{rad+iz}}$ represents the RIB required to be overcome for carbon burn-through. As shown, the RIB for carbon burn-through is critical for I_p ramp-up as it is much higher than the RIB for deuterium burn-through. It should be noted that such a large RIB does not appear for beryllium burn-through, computed with the modified wall-sputtering model which will be discussed in the next section.

4. Wall-sputtering models for the ITER-like wall

One of the main differences of the beryllium wall compared with the carbon wall is that physical sputtering is dominant due to its low threshold energy [16]. It is well known that a physical sputtering yield is a function of incident ion energy. The Bohdansky formula for physical sputtering yield has been given as [17, 18]

$$Y = Q \times S_{\mathrm{n}}(\epsilon) \times g(\delta), \tag{4.1}$$

where Q is yield factor and S_{n} is nuclear stopping cross-section which is given by

$$S_{\mathrm{n}} = \frac{3.441\sqrt{\epsilon}\ln\epsilon + 2.718}{1 + 6.355\sqrt{\epsilon} + \epsilon(6.882\sqrt{\epsilon} - 1.708)}. \tag{4.2}$$

ϵ is defined to be E_0/E_{TF} where E_0 and E_{TF} are the ion wall-impacting energy and the Thomas–Fermi energy, respectively [17, 18]. Assuming a typical sheath formation of negative

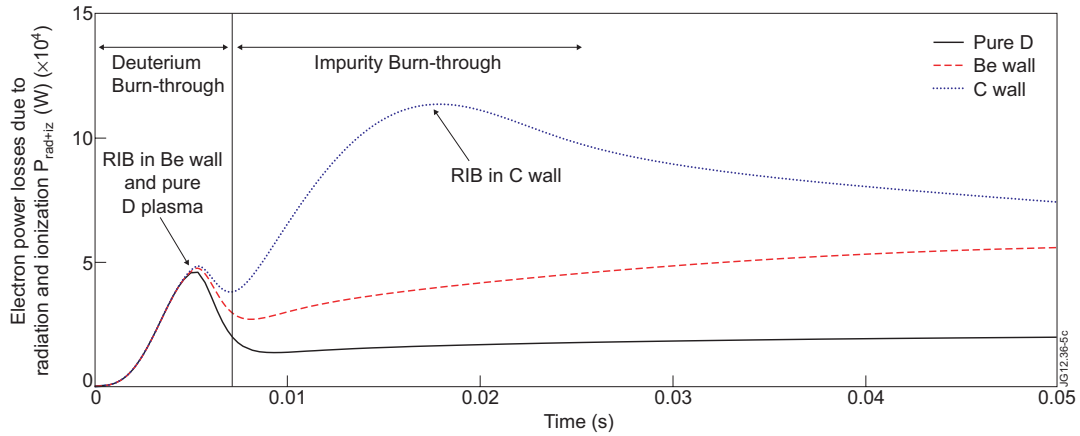

Figure 5. DYON simulation results for a pure deuterium plasma or with wall-sputtering models, i.e. carbon wall or beryllium wall. Each line indicates the electron power losses due to the radiation and ionization: carbon wall (dotted blue), beryllium wall (dashed red) and pure deuterium plasma (solid black). In the case of the carbon wall, the first peak (mainly from deuterium radiation) is much smaller than the second peak, which results from carbon impurities.

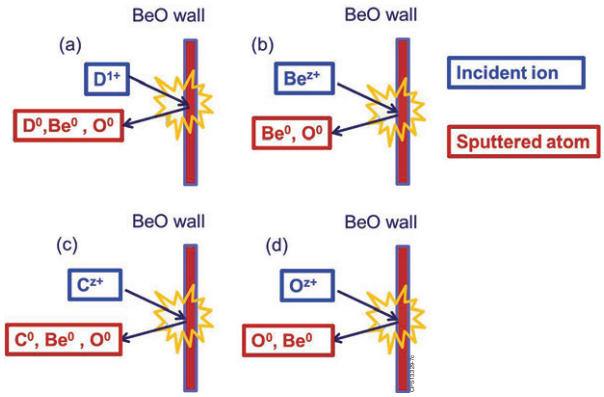

Figure 6. Wall-sputtering and recycling models used in DYON simulations with the ITER-like wall.

potential at the wall [19], the ion wall-impacting energy E_0 can be calculated as $2kT_i + 3kT_e$. That is, the ions have $2kT_i$ of thermal energy when entering the sheath edge (i.e. ion heat transmission coefficient $\gamma_i = 2$), and the ion's energy gain within a sheath is approximately $3kT_e$. The function $g(\delta)$ is defined to be

$$g(\delta) = (1 - \delta^{2/3})(1 - \delta)^2, \tag{4.3}$$

where δ is defined to be E_{th}/E_0 [19]. E_{th} indicates the threshold energy for physical sputtering.

Although there was a small air leak ($\sim 1.5 \times 10^{-6}$ Torr m^{-3} s^{-1}) in JET during the 2011/2012 experimental campaigns with the ITER-like wall, the oxygen level in the residual gas in the vacuum vessel remained lower than in JET with the carbon wall [20]. This implies the oxygen in the air forms a BeO monolayer on the wall. Figure 6 describes the wall-sputtering models used in the DYON simulation for the ITER-like wall. Deuterium, carbon, oxygen and beryllium ions are modelled to be incident ions on the BeO wall (or pure Be wall), resulting in Be (and O) sputtering due to the wall erosion. Since the threshold energy of the tungsten divertor significantly exceeds the range of incident ion energy during the burn-through phase, (e.g. E_{th} of tungsten is 220 eV with D ion bombardment [19]), tungsten sputtering is not taken into account here. The sputtering yield is subject to the oblique angle of incident ions. However, it is difficult to find the effective oblique incidence angle for 0D simulations. In addition, a rapid evolution of the field line angles or even the magnetic geometry during plasma formation from open to closed field lines makes it difficult to assess the incidence angle. For a starting point of this study, we assume normal incidence. In this case, the Bohdansky formula agrees well with more sophisticated models, such as TRIM [21].

The BeO layer contacting the plasma (mainly at the limiter area) would be eroded by the plasma. It is assumed that the surface of the Be wall is oxidized first, and the BeO layer is removed by ion bombardments after a certain erosion period, changing the BeO wall to the pure Be wall. Including the effects of the BeO layer erosion, the impurity influx due to the physical sputtering is modelled as

$$\Gamma^0_{\mathrm{Be,in}} = V_p \sum_A \sum_{z \geqslant 1} (C_{\mathrm{BeO}} Y_A^{\mathrm{BeO}} + (1 - C_{\mathrm{BeO}}) Y_A^{\mathrm{Be}}) \frac{n_A^{z+}}{\tau_p} \tag{4.4}$$

$$\Gamma^0_{\mathrm{O,in}} = V_p \sum_A \sum_{z \geqslant 1} C_{\mathrm{BeO}} Y_A^{\mathrm{BeO}} \frac{n_A^{z+}}{\tau_p} \tag{4.5}$$

$$\Gamma^0_{\mathrm{D,in}} = V_p Y_D^D \frac{n_D^{1+}}{\tau_p} \tag{4.6}$$

$$\Gamma^0_{\mathrm{C,in}} = V_p \sum_{z \geqslant 1} Y_D^D \frac{n_C^{z+}}{\tau_p}, \tag{4.7}$$

where superscript and subscript of Y indicate the sputtered (or recycled) species and an incident ion, respectively. For example, Y_D^{BeO} is the BeO sputtering yield due to D ion bombardment. C_{BeO} is defined as the BeO erosion coefficient, which is used to model the transition from BeO wall to Be wall at the end of the BeO layer erosion time τ_{erosion}. C_{BeO} is 1 before τ_{erosion} (ms) and decreases to 0 after τ_{erosion}. τ_{erosion} is adjusted to be 60 ms based on obtaining agreement of the synthetic data for bolometry and Be^{1+} PM tube signals against the measured data. The parameters required to calculate physical sputtering yields of the BeO wall (or pure Be wall) are given in table 2.

The incident ions are also recycled as neutrals at the wall with a fraction, called the recycling coefficient. It is observed

Table 2. Parameters for the physical sputtering yield of beryllium in the ITER-like wall [19, 23].

Incident ion / target	D^{1+}/Be	D^{1+}/BeO	Be^{z+}/Be	C^{z+}/Be	O^{z+}/Be
E_{th} eV	10	29	23	40	70
E_{TF} eV	282	444	2208	4152	6970
Q	0.22	0.13	0.77	1.6	1.3

at JET that during the plasma burn-through phase the carbon wall releases deuterium into the plasma, while the beryllium-wall pumps them from the plasma [5]. Hence, for DYON simulations with the carbon wall, an exponential decay model was used i.e. $Y_D^D = 1.1 \rightarrow 1$. However, the deuterium recycling coefficient with the ITER-like wall is modelled to grow and approach 1 during the plasma burn-through phase. That is, the exponential growing model is used for DYON simulations with the ITER-like wall i.e. $Y_D^D = 0.9 \rightarrow 1$. This is consistent with the outgassing observed after discharges with the ITER-like wall [22].

5. ITER-like wall simulations and comparison with the JET data

5.1. Validation of the new models

The recent installation of the ITER-like wall at JET enables us to validate the new sputtering (or recycling) models at the beryllium wall. For the validation of the new models, one typical discharge in JET has been selected (#82003), and compared with the DYON simulation results. Figure 7 shows the DYON simulation results and the JET data with the ITER-like wall. The required input parameters for the DYON simulation, i.e. prefill gas pressure, loop voltage, plasma major and minor radius, toroidal magnetic field and additional fuelling, are obtained from the measured data. The parameters given to perform the simulation are summarized in table 3.

The plasma current in the DYON simulation is in good agreement with the JET data. As shown in figure 7(*b*), the toroidal loop voltage decreases abruptly at 0.1 s due to the pre-programmed use of a switching network to reduce the voltage from the ohmic transformer, a typical operation scenario at JET. This results in the sharp decrease in the I_p ramp-up rate around 0.1 s in figure 7(*a*). The measured loop voltage is used as an input for the simulations.

Figure 7(*c*) shows the total radiation power loss. In the simulations, the temporal behaviour of the radiation barrier is used to adjust $\tau_{erosion}$. The synthetic bolometry data can be well reproduced with $\tau_{erosion} (= 60\,\text{ms})$. For this simulation, the initial carbon content $n_C^0(0)$ is assumed to be 0.5% of prefill deuterium atoms $n_D^0(0)$. As will be discussed later, the assumption of $n_C^0(0)$ has a small contribution to the magnitude of the radiation barrier. Also, both $\tau_{erosion}$ and $n_C^0(0)$ do not have a significant influence on the evolution of other plasma parameters, i.e. $I_p(t)$, $T_e(t)$ and $n_e(t)$.

The T_e and n_e in the simulations and the Thomson scattering data approach similar values, but they have a discrepancy before 0.2 s. The discrepancy is due to the limitations of the Thomson scattering diagnostic, which can have significant error bars during the low density phase such as the plasma burn-through phase. The interferometry data show a better agreement with the density in the simulations during this early phase, as shown in figure 7(*e*).

As ionization of deuterium and impurities proceeds, the photomultiplier tube data have a peak for each specific line emission, which is emitted from the deuterium atom or impurity ion in a certain charge state. Synthetic data of photomultiplier tube $I_{A^{z+}}$ can be calculated with the plasma parameters (n_e, n_A^{z+} and T_e) obtained by the DYON simulation as

$$I_{A^{z+}} = n_e n_A^{z+} \mathcal{PEC}_{A^{z+}}(n_e, T_e)\,\text{p}\,\text{m}^{-3}\,\text{s}^{-1}, \qquad (5.1)$$

where $\mathcal{PEC}_{A^{z+}}(n_e, T_e)$ is a photon emissivity coefficient, which is a function of electron density and temperature. Here, A and $z+$ indicate the corresponding particle species and the charge state, respectively. The photon emissivity coefficients are obtained from the ADAS package [10]. The synthetic volume emission of Be^{1+}(527 nm), D^0 (D alpha) and C^{2+} (465 nm) are compared with the measured photon flux in figures 8(*a*)–(*c*). The temporal behaviour of the peaks in the synthetic data is coincident with the measured data. This implies that the ionization process of deuterium and impurities is reproduced correctly in the DYON simulations.

5.2. Beryllium sputtering in the ITER-like wall

In the DYON simulations, the first radiation peak for Be^{1+} is reproduced showing a very good temporal agreement with the photomultiplier tube data in figure 9(*a*). However, the first radiation peak is removed when the initial beryllium content is not assumed in the simulations, as shown in figure 9(*b*). This implies that the first radiation peak results from the initial beryllium content rather than physical sputtering. These particles are probably the beryllium atoms bonded weakly at the wall due to the migrations of beryllium in the vacuum vessel during previous experiments.

The secondary radiation peak in the photomultiplier tube data for Be^{1+} is observed at around 0.07 s, as shown in figure 8(*a*). It should be noted that such a secondary radiation peak does not appear for D^0 and C^{2+} in figures 8(*b*) and (*c*). This is because the secondary radiation peak results from the wall-sputtering rather than the initial impurity content. Wall-sputtering can occur only if the incident ion energy exceeds the threshold energy. This implies that the beryllium sputtering is delayed until the wall-impacting energy, $2kT_i + 3kT_e$, exceeds the threshold energy. The secondary radiation peak is reproduced with the physical sputtering model, showing a good temporal agreement in figure 9(*a*). Figure 9(*b*) shows the DYON simulation results without the physical sputtering model. The secondary radiation peak does not appear without the physical sputtering model. This leads to the conclusion that the secondary radiation peak results from the delayed physical sputtering.

It is observed in many laboratory plasmas that the surface of beryllium tiles are easily oxidized [23–25]. The high affinity of Be to O tends to result in the BeO layer on the wall, which has higher surface binding energy than the pure beryllium wall [23]. In table 2, the threshold energy of a deuterium incident ion for the physical sputtering on the BeO layer is 29 eV, which is much higher than that on a pure beryllium wall, 10 eV. The higher surface binding energy in the BeO layer makes the physical sputtering more difficult than in the pure beryllium wall. The simulation results using the different parameters

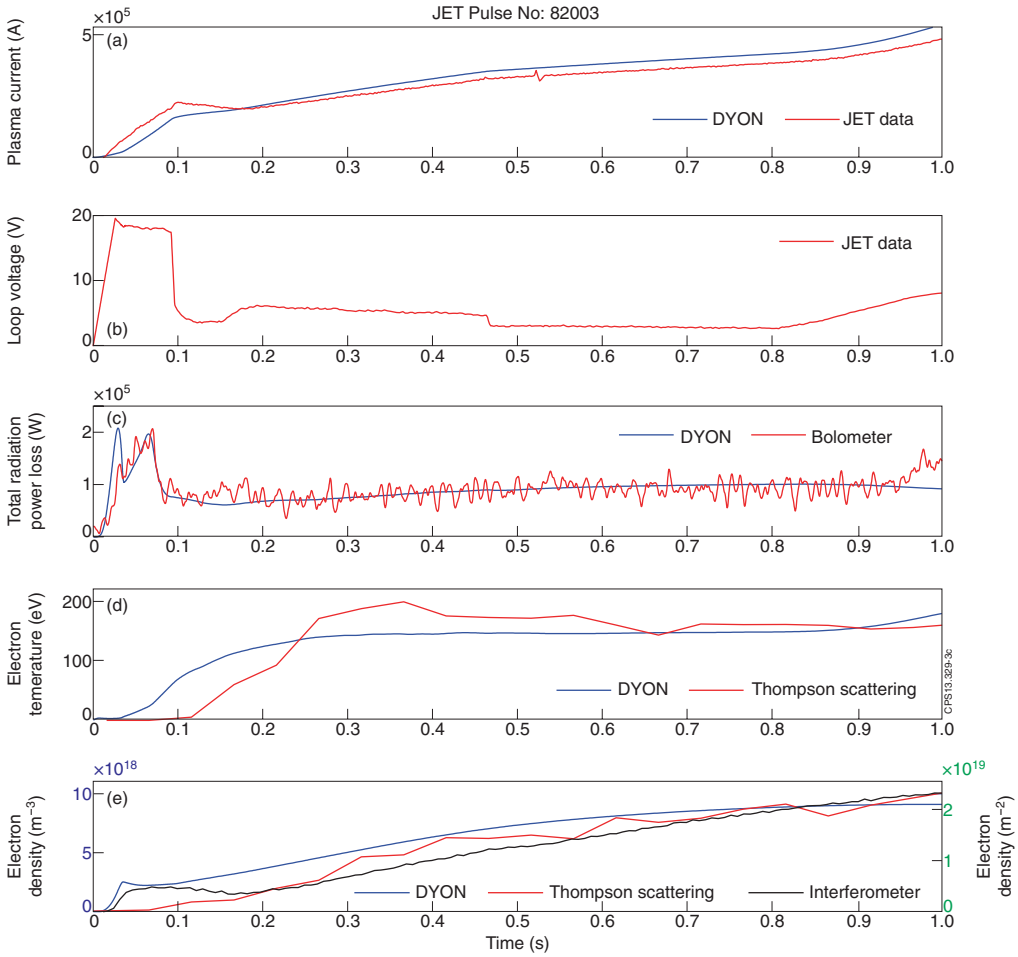

Figure 7. DYON simulation results with the new models for the ITER-like wall and JET data. (*a*) Plasma current, (*b*) loop voltage, (*c*) total radiation power (bolometry), (*d*) electron temperature (Thomson scattering), (*e*) electron density (Thomson scattering and interferometry). The red lines (and the black line in (*e*)) indicate JET data for #82003, and the blue lines are the corresponding DYON simulation results. The condition given for the simulations is in table 3.

Table 3. Plasma parameters assumed for the DYON simulation (#82003) in the ITER-like wall.

Plasma parameters	Input values
Toroidal magnetic field B_ϕ	2.7 T
Vertical magnetic field B_v	0.001 T
Initial plasma current $I_p(0)$	0 A
Initial eddy current $I_{MK2}(0)$	0 A
Initial electron temperature $T_e(0)$	1 eV
Initial ion temperature $T_i(0)$	0.03 eV
Prefilled gas pressure $p(0)$	4.3135×10^{-5} Torr
Initial deuterium atom density $n_D^0(0)$	$2.78 \times 10^{22} \times p(0)$ Torr
Initial degree of ionization $\gamma_{iz}(0)$	0.002
Initial Be content $n_{Be}^0(0)$	$0.01 \times n_D^0(0)\ m^{-3}$
Initial C content $n_C^0(0)$	$0.005 \times n_D^0(0)\ m^{-3}$
Initial O content $n_O^0(0)$	$0\ m^{-3}$
Y_D^D	$c_1 = 0.9, c_2 = -0.1, c_3 = 0.1$ in equation (5.2)
Fuelling efficiency	10%
PSI model	Physical sputtering with BeO wall
Plasma major radius $R(t)$	EFIT ($R(0) = 3.0381$ m)
Plasma minor radius $a(t)$	EFIT ($a(0) = 0.08519$ m)
Internal inductance l_i	0.5
Loop voltage $U_l(t)$	Measured in JET
Vacuum vessel volume	$100\ m^{-3}$

for BeO and Be are compared in figures 9(*a*) and (*c*). The secondary radiation peak in figure 9(*c*) occurs much earlier, showing a deviation from the measured value.

Due to the erosion of the BeO layer, the BeO sputtering model is switched to the Be sputtering at $\tau_{erosion}(\approx 60$ ms). Figure 9(*d*) shows BeO sputtering without switching to Be sputtering, i.e. no BeO erosion model. The secondary peak shows a reasonable temporal agreement with the measured, but it decreases slowly, without the sharp peak observed in the measured and the simulated with the erosion model. Moreover, in this case the radiation resulting from oxygen would be much higher than measured.

Based on the frequency of the fluctuating radiation, it is found that the third peak around 100–200 ms in the photomultiplier tube data for Be^{1+} is probably due to an MHD instability in the plasma, which is not modelled in the DYON simulation. Since a detailed investigation on the MHD instabilities is beyond the scope of this paper, this is not discussed further here.

5.3. *Deuterium recycling coefficient*

The initial deuterium recycling coefficient $Y_D^D(0)$ is subject to the wall condition, and $Y_D^D(t)$ approaches 1 as the deuterium

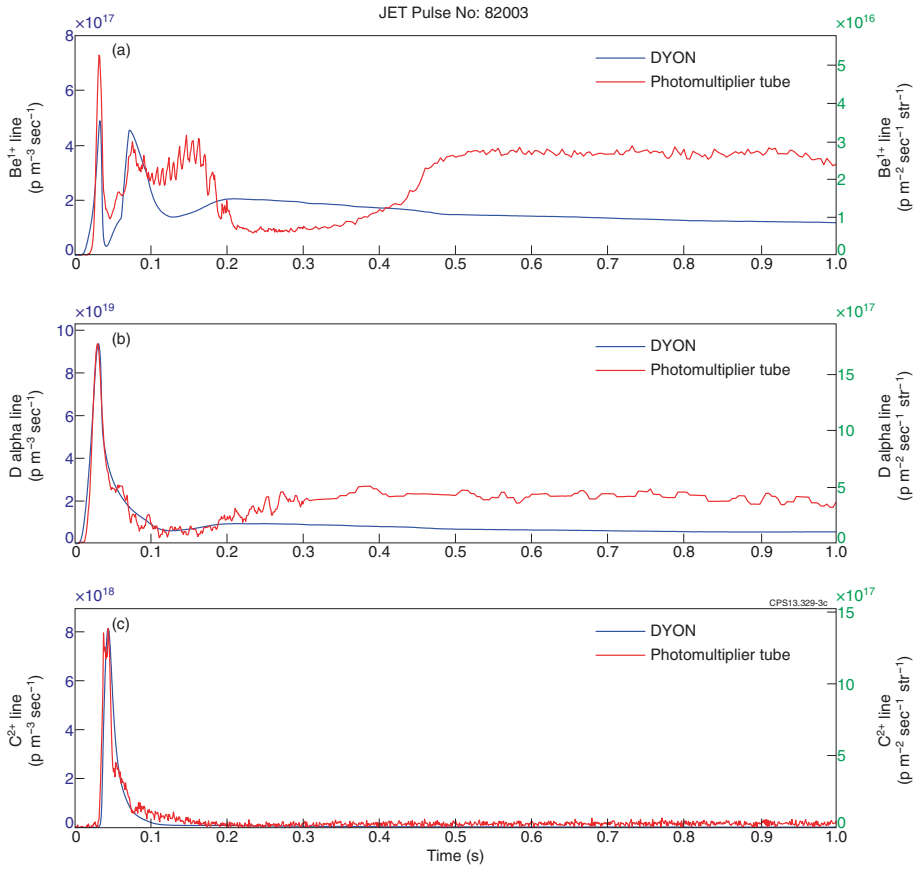

Figure 8. The measured photomultiplier tube data and the synthetic photomultiplier tube data: (*a*) number of photons emitted from Be^{1+} (527 nm), (*b*) number of photons emitted from D^0 (D alpha) and (*c*) number of photons emitted from C^{2+} (465 nm). The red lines are the photomultiplier tube data in JET for #82003, and the blue lines are the synthetic data, calculated by DYON simulations.

inventory at the wall saturates. The varying deuterium recycling coefficient $Y_{\rm D}^{D}(t)$ can be modelled by [11]

$$Y_{\rm D}^{D}(t) = c_1 - c_2(1 - \exp\left(-\frac{t}{c_3}\right)). \tag{5.2}$$

$Y_{\rm D}^{D}(t)$ is adjusted by the combination of constants c_1, c_2 and c_3. In order to test whether $Y_{\rm D}^{D}$ is growing or decaying during the plasma burn-through phase, the constants are assumed to be $c_1 = 0.9$, $c_2 = -0.1$ and $c_3 = 0.1$ for the growing model, and $c_1 = 1.1$, $c_2 = 0.1$ and $c_3 = 0.1$ for the decay model.

Figure 10 shows the different simulation results between the two sets of parameters used. The decay model implies additional release of deuterium atoms during the plasma burn-through phase. This results in a very high electron density in the simulation compared with the Thomson scattering data in figure 10(*a*). The discrepancy is reduced by the growing model as indicated by the blue solid lines in figure 10(*a*). This implies that some portion of incident deuterium ions are retained at the wall rather than being recycled. Based on this, the growing model for recycling is used for the simulations with the ITER-like wall in figure 7. It should be noted that for the carbon-wall simulations the DYON simulation results with the decay model showed better agreement with the JET data [11].

Figure 10(*b*) gives another indication that the growing model is required for the ITER-like wall. The synthetic data for the D alpha line using the growing model shows very good agreement against the measured value for 0–0.2 s. However, with the decay model, the synthetic data deviate significantly from the measured value as shown in figure 10(*b*). This gives a confidence on the fact that such additional release of deuterium atoms during the plasma burn-through phase is not probable in the ITER-like wall.

5.4. Gas fuelling

One of the main differences in the JET operation scenario with the ITER-like wall is the use of additional gas fuelling around 0.1 s. This is to compensate for the gas pumping effect at the wall as seen with the new wall [5]. The additional gas fuelling influences on the particle balance of deuterium atoms [11],

$$\frac{{\rm d}n_{\rm D}^{0}}{{\rm d}t} = \frac{1}{\gamma_n^{D} V_{\rm V}}(V_{\rm p}\mathcal{R}_{\rm D,rec}^{1+\to 0} n_{\rm e} n_{\rm D}^{1+} - V_n^{D}\mathcal{R}_{\rm D,iz}^{0\to 1+} n_{\rm e} n_{\rm D}^{0} - V_n^{D}\sum_{I}\sum_{z\geqslant 1}\mathcal{R}_{I,cx}^{z+\to(z-1)+} n_{\rm D}^{0} n_I^{z+}) + \frac{\Gamma_{\rm D,in}^{\rm total}}{\gamma_n^{D} V_{\rm V}}, \tag{5.3}$$

where the total influx of deuterium atoms $\Gamma_{\rm D,in}^{\rm total}$ is

$$\Gamma_{\rm D,in}^{\rm total} = V_{\rm p}\frac{Y_{\rm D}^{D} n_{\rm D}^{1+}}{\tau_{\rm D}} + \Gamma_{\rm D,in}^{\rm eff}. \tag{5.4}$$

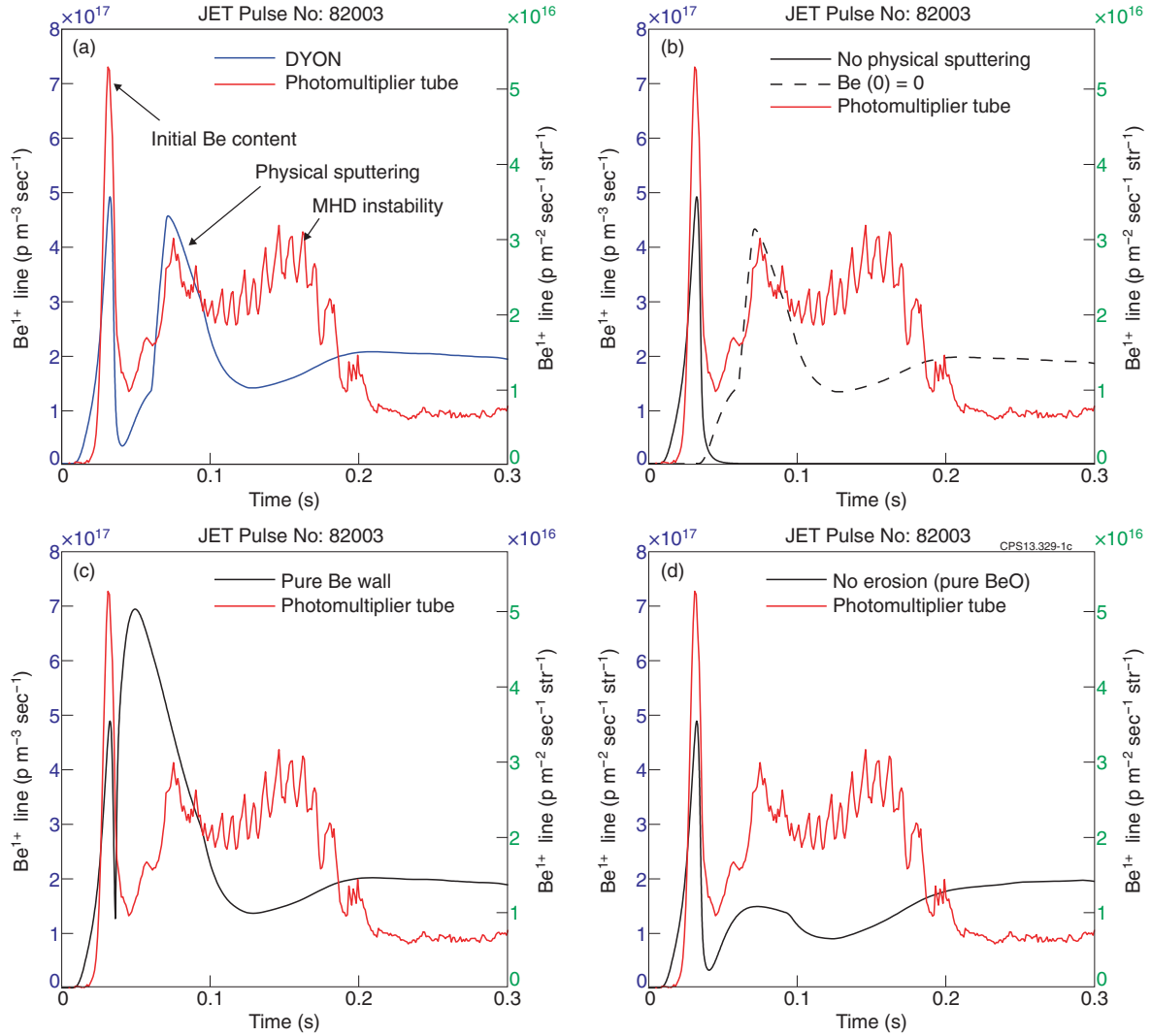

Figure 9. These figures compare the photomultiplier tube data (Be^{1+} (527 nm)) between the measured data and the synthetic data, and show the significance of the new models used in the DYON simulations. The red solid lines are the photomultiplier tube data in JET for #82003. The blue solid line in (*a*) is the synthetic data with the condition given in table 3 (i.e. with the physical sputtering model on the BeO layer, the erosion model of the BeO layer and initial Be content). The black dashed line and solid line in (*b*) are without initial Be content or any physical sputtering model, respectively. The black solid line in (*c*) is for the pure Be wall. The black solid line in (*d*) is without the erosion model of the BeO layer, i.e. the continuous BeO layer.

The first term in equation (5.4) is the influx of the deuterium atoms recycled at the wall, and the second term is the additional gas fuelling $\Gamma^{\rm eff}_{\rm D,in}$, which was not included for the carbon-wall simulations. In the simulations for the ITER-like wall, $\Gamma^{\rm eff}_{\rm D,in}$ is modelled as

$$\Gamma^{\rm eff}_{\rm D,in} = \psi_{\rm puffing}\Gamma^{\rm GIM}_{\rm D,in}, \tag{5.5}$$

where $\Gamma^{\rm GIM}_{\rm D,in}$ is obtained from the data of the gas injection modules in JET [26] and $\psi_{\rm puffing}$ is a fuelling efficiency. The gas injection module used for the fuelling at 0.1 s is located on the top of Oct 8 in JET, and the four main pumping ports, two neutral beam injection (NBI) ports and one lower hybrid (LH) ports are on the outer midplane of the vessel. Since a significant fraction of the injected gas is pumped out immediately rather than being ionized, the fuelling efficiency must be evaluated for the effective influx of deuterium atoms. Figure 11 shows the differences in the simulation results when assuming 30% and 0% for the fuelling efficiency $\psi_{\rm puffing}$. Since gas injection is applied from 0.1 s as can be seen in figure 11(*a*), the simulation results do not show discrepancy until then. However, the electron density with 30% fuelling efficiency increases excessively from 0.1 s onwards as shown in figure 11(*b*). In contrast, without the fuelling model i.e. 0% fuelling efficiency, the electron density in figure 11(*b*) is much lower than Thomson scattering data. By scanning the fuelling efficiency, it has been found that the simulation results with 10% fuelling efficiency agree well with the JET data. Based on this, 10% fuelling efficiency is assumed for the simulations in figures 7 and 8.

5.5. *Initial carbon content*

Although all CFC tiles have been removed from the plasma-facing components in the ITER-like wall, the C^{2+} line emission is still observed in the ITER-like wall JET data as shown in

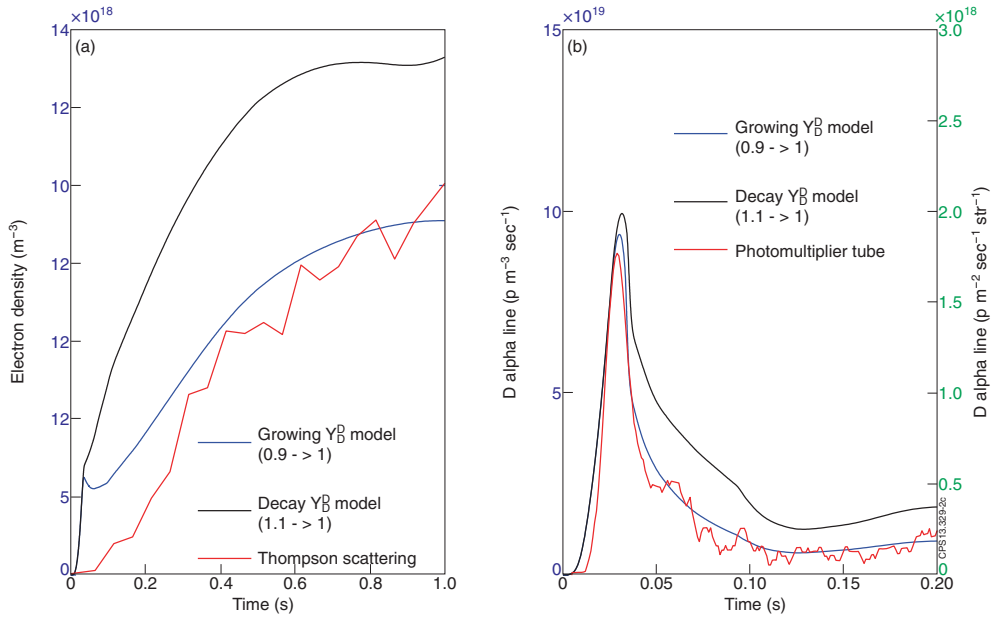

Figure 10. The figures show the effects of the deuterium recycling coefficients. (*a*) Electron density, (*b*) number of photons emitted from D^0(D alpha) (465 nm). The red lines are (*a*) Thomson scattering data, (*b*) the measured photomultiplier tube data in JET (#82003). The blue and black lines are the DYON simulation results with the growing model or decay model of Y_D^D, respectively.

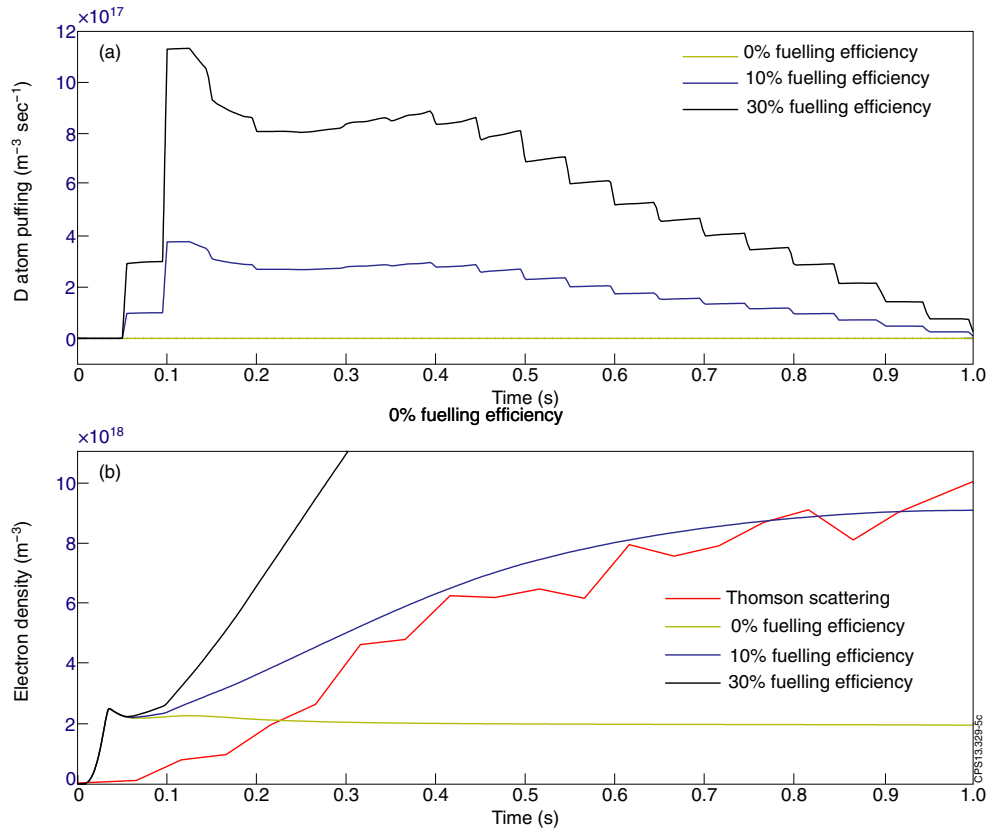

Figure 11. The figures show the effects of fuelling efficiency. (*a*) D atom puffing with the assumed fuelling efficiency (black 30%, blue 10% and green 0%), (*b*) electron densities, obtained by DYON simulation (black 30%, blue 10% and green 0%) and measured by Thomson scattering (red) in JET (#82003).

figure 8(*c*). This requires the assumption of an initial carbon content $n_C^0(0)$ for the ITER-like wall simulations.

The total carbon content assumed at plasma initiation is between 0% and 1% of the prefill deuterium atom density $n_D^0(0)$; $n_C^0(0) \sim 10^{16}\,\mathrm{m}^{-3}$. This value is lower than the carbon content during the main heating phase of JET plasmas, which is reported [27] as 0.1–0.2% of the plasma density (in the range 10^{19}–$10^{20}\,\mathrm{m}^{-3}$) during the heating phase. Figure 12(*a*)

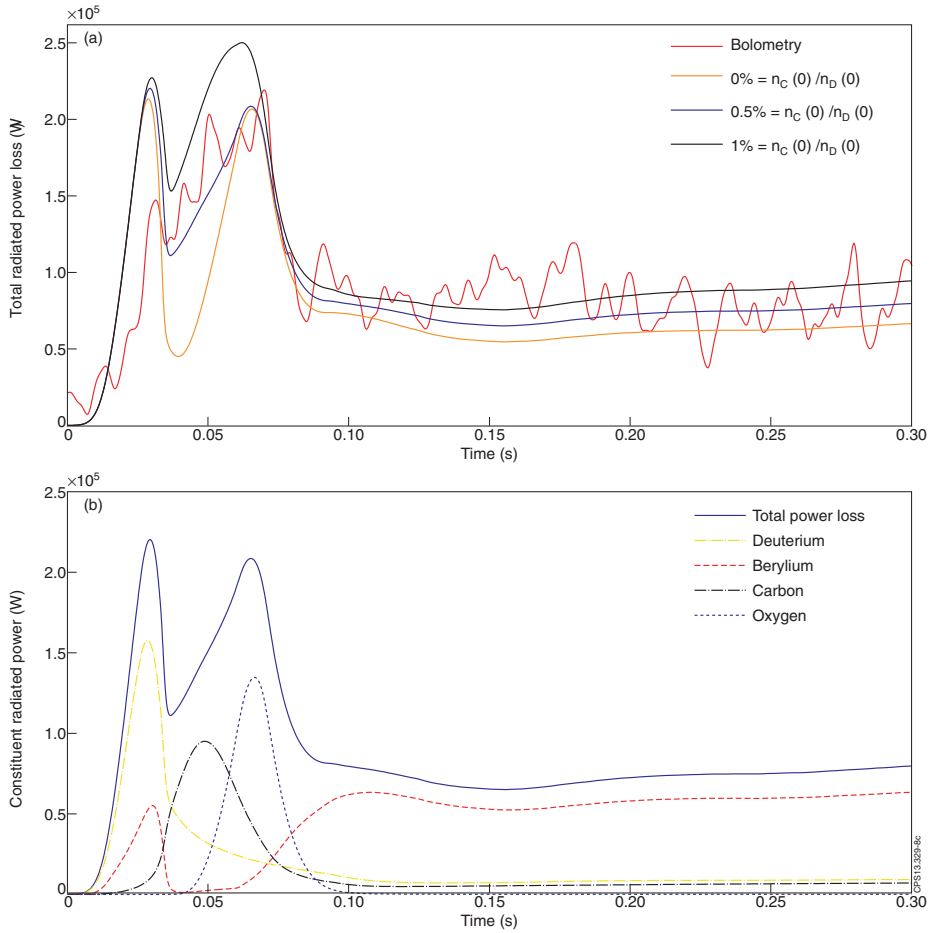

Figure 12. The figures show the effects of $n_c^0(0)$ on the radiation barrier and the constituent radiated power. (*a*) Bolometry data (red) in JET (#82003), and the simulated radiated power in the DYON simulations (solid black 1%, solid blue 0.5% and solid green 0% of $n_c^0(0)$). (*b*) The constituent radiated power (solid blue: total radiated power, dashed red: Be, dashed green: D, dashed black: C, dashed blue: O). For the simulation in (*b*), the $n_c^0(0)$ is assumed to be 0.5%, as given for the simulation in figures 7 and 8.

shows the total radiation power loss in the simulations with $n_C^0(0)$. Here, the initial carbon content $n_C^0(0)$ is assumed to be 0%, 0.5% or 1% of the initial deuterium atom density $n_D^0(0)$, respectively. As shown in figure 12(*a*), without $n_C^0(0)$, the synthetic radiation barrier deviates from (below) the bolometry data. The magnitude of the total radiation power loss in the simulation with 1% $n_C^0(0)$ exceeds the peak of the bolometry data. However, in the case of the simulation with 0.5% $n_C^0(0)$, the radiation barrier shows good agreement. Based on this, 0.5% $n_C^0(0)$ is assumed in the simulations.

Figure 12(*b*) shows the constituent radiated power losses in the case of the simulation with 0.5% $n_C^0(0)$. It can be seen that the radiation is dominated in turn by the radiated power loss from deuterium, carbon, oxygen and beryllium. The radiated power loss due to beryllium is not significant in the radiation barrier during the plasma burn-through phase.

6. Operation space for plasma burn-through in JET

Figure 13 compares the Townsend criterion and the criterion for plasma burn-through. The cyan lines in figure 13 are the minimum electric field for electron avalanche $E_{\text{avalanche}}$ for two effective connection lengths $L_f (= 500$ and 2000 m) in JET, drawn analytically using the Townsend criterion in equation (1.1). The Townsend criterion shows that there is an optimum range of the prefill gas pressure at which the lowest toroidal electric field is available for electron avalanche. However, for successful tokamak start-up, operation space is not only determined by the Townsend criterion, but also by the criterion for plasma burn-through. The black, red and blue lines in figure 13 represent the required electric field for plasma burn-through E_{Burn} without or with impurities, obtained using DYON simulation results. The wall-sputtering models described in sections 3 and 4 are used for the DYON simulations. Plasma parameters assumed for the DYON simulation are indicated in table 1.

The criterion for plasma burn-through is computed from the numerical simulations using several assumptions, subject to wall conditions and operation scenario. However, the simulation results provide informative insight on the operation space. As shown in figure 13, the required electric field for plasma burn-through increases monotonically as prefill gas pressure rises since the RIB is greater at a high prefill gas pressure. This monotonic increase with prefill gas pressure is consistent with equation (2.15), which is analytically derived for deuterium burn-through.

If the effects of the impurities from the wall are included, the required electric field for plasma burn-through increases,

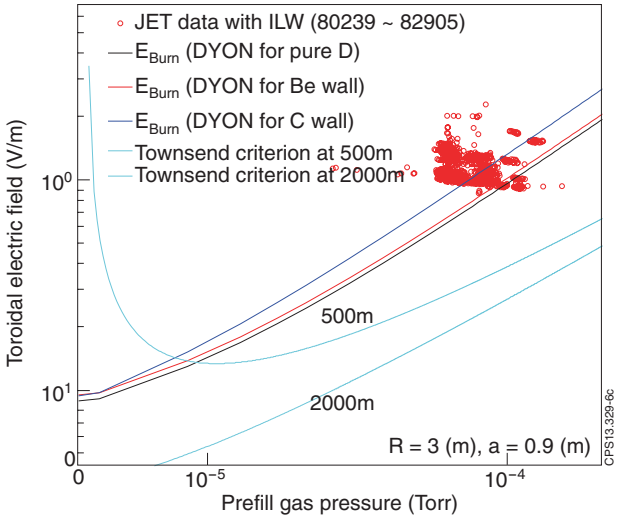

Figure 13. The cyan lines show the Townsend criterion at different effective connection lengths, as indicated with 500 m and 2000 m, respectively. The black, red and blue lines indicate the criterion for plasma burn-through, i.e. the minimum electric field for plasma burn-through in the case of a pure deuterium plasma (black), beryllium wall (red) and carbon wall (blue), respectively. The wall-sputtering models described in sections 3 and 4 are used for the simulations, and the required plasma parameters are given by table 1. The area above both the burn-through criterion and Townsend criterion represents the operation space available for successful start-up in JET. The red circles indicate the successful plasma burn-through in JET experiments with ITER-like wall (#80239–82905).

thereby reducing the operation space available. As can be seen in figure 5, the RIB for carbon burn-through is much greater than for deuterium burn-through. Hence, the required loop voltage in the carbon wall is significantly higher than for a pure deuterium plasma. This results in the smaller operation space available in the carbon wall as shown in figure 13. However, the RIB for beryllium burn-through is not significant in figure 5. With the beryllium wall, the critical RIB to be overcome is for deuterium rather than for beryllium as long as other impurities are not significant [28]. This implies that lower loop voltage can be used for plasma burn-through in the ITER-like wall, i.e. larger operation space available compared with the carbon wall as shown in figure 13. The red circles in figure 13 show successful plasma burn-through in JET experiments with the ITER-like wall (#80239–#82905). It should be noted that most successful shots are located above the red line, which is the criterion for plasma burn-through with the beryllium wall.

The criterion for plasma burn-through in figure 13 can change with different assumptions in the DYON code. That is, the increase in required loop voltage with increasing prefill gas pressure is steeper for higher recycling coefficient (or sputtering yield) or for higher ratio of the effective vessel volume to the plasma volume, i.e. V_V/V_p. In tokamaks, the recycling coefficients and the sputtering yields vary due to the effects of deuterium retention and impurity migration in the wall. In addition, V_V/V_p, which is related to dynamic neutral gas fuelling from the ex-plasma volume, is also varying according to the operation scenario. Hence, to find the precise operation space using the simulations, the information on the wall conditions and operation scenario in each shot should be specified.

7. Discussion

The investigation of plasma burn-through has been published only with 0D simulations [7, 11, 29, 30]. Since the closed flux surfaces (CFSs) are not established yet during the plasma burn-through phase at low plasma current, a 2D approach of numerical simulation is extremely difficult. Fortunately, the results of DYON simulations (also 0D) show good agreement with JET data. This implies the assumption of a uniform temperature and density in a numerical simulation is reasonable to compute the gross energy and particle balances during the plasma burn-through phase. Probably, this is due to the open field configurations during the plasma burn-through phase. With the open magnetic field lines, the parallel thermal conduction and particle diffusion would be significant. Quantitative investigations on the profile effects of temperature and density will be interesting to confirm this. Regarding the profile of plasma current, a flat current profile is assumed, i.e. $l_i = 0.5$. According to a scan of l_i with the DYON code, the internal inductance does not have a significant effect on the simulation results since most of the power is consumed by ohmic heating.

The synthetic PM tube data are not dependent on the initial electron temperature $T_e(0)$ assumed in the simulations. $T_e(t)$ quickly saturates to the same value in a few milliseconds regardless of the assumed value of $T_e(0)$. It has been checked in the simulations, starting with $T_e(0) = 1$, 3 and 5 eV.

We assume fully dissociated D gas, and this is a reasonable assumption for $T_e(0) = 1$ eV, the initial condition in the simulation. The dissociation energy per D atom P_{dis} is just 2.26 eV. Compared with D ionization energy 13.6 eV, this is small. Moreover, radiation power loss is much greater than D ionization energy, i.e. $P_{rad} > P_{iz} > P_{dis}$. This has been checked in the simulations by adding 2.26 eV to D ionization energy; the simulation results did not show any visible difference. Hence, the D dissociation energy can be ignored in the simulation.

One of the underlying assumptions in the simulations is that all deuterium atoms are accessible to the plasma. This implies the vessel volume determines the neutral influx into the plasma. However, deuterium atoms in large ports for diagnostics or additional heating and near pumping ports are impeded to approach the plasma. For example, the neutral particles in the cryogenic pumping chamber for the NBI system (i.e. V_{NBI}) cannot access the main plasma. Hence, V_{NBI} should not be included in V_V. The initial peak of bolometry data is proportional to the number of deuterium atoms in the vessel. Comparing the reproduced bolometry data with the measured, we could find the effective vessel volume V_V is around 100 m^{-3} in JET, although the total volume of the vacuum vessel is 189 m^{-3}.

The formula for impact ion energy (i.e. $E_0 = \gamma_i kT_i + 3kT_e$, where $\gamma_i = 2$) is good enough for the scope of this paper, and the simulation results match well with experimental data. However, it should be noted that the formula does not include all physical processes for computing the impact ion energy. Due to the pre-sheath acceleration, the ions at the sheath edge

do not have Maxwellian velocity distribution. This results in different γ_i depending on the model assumed ($\gamma_i \approx 1.5$–2.93) [31]. For more accurate calculation of γ_i it would be needed to solve full kinetic equations using the distorted energy distribution of the ions. However, the calculation has not been well established yet. The pre-sheath energy gain is ignored in the adopted formula since it is assumed to be small compared with the uncertainty of γ_i and the sheath energy gain. However, the wall impact energy of impurities can be higher than the value calculated using the adopted formula if impurity flow velocity is equal to the ion sound speed C_s ($= \sqrt{\frac{T_e+T_i}{m_D}}$). For example, in the case of Be^{1+} in isothermal plasma ($T_e = T_i$), the wall impact energy is

$$E_0^{Be^{1+}} = 0.5kT_e + \frac{1}{2}m_{Be}C_s^2 + (2kT_i + 3kT_e) \approx 10kT_e, \quad (7.1)$$

where the first term is due to pre-sheath acceleration, the second term is due to the sound speed equilibrium and the third term is due to temperature equilibration plus sheath-acceleration. The result is almost twice as high as the formula ($E_0 = 2kT_i + 3kT_e$). Fortunately, the formula used in the simulations is still valid since the majority of impacting ions are deuterium in the simulation.

The deuterium recycling coefficient has a significant influence on plasma burn-through and the dynamics of the deuterium recycling coefficient is different for the carbon wall and the ITER-like wall. This probably results from the different retention of deuterium at the wall. In the carbon wall, deuterium is retained especially after disruptions, so that the simulation results using the decay model of Y_D^D match well with JET data [11]. However, in the ITER-like wall, the DYON results using the growing model of Y_D^D show good agreement with JET data. This might be due to the fact that most of the attached deuterium, even after the disruption event, are easily removed by pumping between discharges [32] (typically 30–40 min in JET).

Deuterium fuelling has a significant effect, and it should be confirmed for ITER simulations. However, it might not be a critical issue for plasma burn-through if the fuelling is pre-programmed after about 100 ms, when plasma burn-through is completed. As shown in figure 11, fuelling does not result in differences on plasma parameters during the plasma burn-through phase.

As shown in figure 12(*b*), the radiation barrier in the ITER-like wall simulations is dominated by deuterium, carbon and oxygen. The simulation results with 0.5% $n_C^0(0)$ show good agreement with experimental data. However, the simulation results with 0% and 1% $n_C^0(0)$ still show reasonable agreement in the other plasma parameters, i.e. $I_p(t)$, $T_e(t)$ and $n_e(t)$.

Plasma initiation in JET experiments with the ITER-like wall is very reliable. According to an experimental characterization of plasma formation with the ITER-like wall [5], the failures during the plasma burn-through phase, that usually occurred with the carbon wall (mostly after disruptions), were not observed with the ITER-like wall. This implies that the plasma parameters during the burn-through phase, including the radiated power losses from impurities, are not likely to vary significantly in each shot, even after disruption events. Hence, the validation of #82003 is representative of plasma burn-through simulations for other shots with the ITER-like wall.

In ITER, oxidation of the beryllium surface might be much less than in JET, due to the much longer plasma pulses. Also, the initial carbon content would be much reduced if the first divertor is made solely of tungsten. On the other hand, due to the use of seeding gases, there should be various impurities, e.g. Ar, Ne or N. Hence, modelling impurity seeding in the simulations would be interesting for predictive simulations of ITER. In DYON simulations, RF heating is not included as no RF heating was used for the simulated pulse (# 82003), but RF-assisted start-up is planned in ITER. In order to apply the DYON code to such operations, it is required for development of an RF-heating module. Modification of the points stated above will enable the DYON code to be applied for a predictive simulation of the plasma formation in ITER.

8. Conclusion

In this paper, key physics aspects in the plasma burn-through phase are investigated with the DYON code. The criterion for plasma burn-through is explained with the radiation and ionization barrier (RIB) and the critical degree of ionization $\gamma_{iz}(t_{RIB})$.

For ITER-like wall simulations, the modification of the wall-sputtering model in the DYON code is described in detail, and the simulation results using the modified wall-sputtering models are compared with JET data with the ITER-like wall, and the simulation results show good agreement.

The results of parameter scanning in DYON simulations show that the deuterium recycling coefficient significantly influences the gross energy and particle balance, and the simulation results with the growing model of Y_D^D show good agreement. This implies that during the plasma burn-through phase deuteriums are pumped out by the beryllium wall. Second, the physical sputtering model using the BeO layer erosion model agrees well with the photomultiplier tube data. Third, the radiation barrier in the ITER-like wall is dominated by deuterium and other impurities rather than beryllium. The initial carbon content does not influence other plasma parameters significantly in the simulation results. Fourth, in the case of JET with the ITER-like wall, plasma burn-through is not affected by gas fuelling if the fuelling is pre-programmed after 100 ms.

The required electric field for deuterium burn-through is calculated by the DYON code, and it is compared with the Townsend avalanche criterion. The limitations set by the burn-through criterion will reduce the operational space with respect to those only based on the Townsend criterion for an electron avalanche.

The operation space available for JET is computed for the carbon wall and the ITER-like wall. The impurity effects result in a reduced operation space for the carbon wall compared with a pure deuterium plasma. However, the RIB in the ITER-like wall is not much higher than in a pure deuterium plasma. This results in larger operation space available for successful plasma initiation in the ITER-like wall than in the carbon wall. It is also observed that the prefill gas pressure and toroidal electric field used in successful plasma initiation of JET experiments with the ITER-like wall are located within the operation space computed for the ITER-like wall.

Acknowledgments

This research was funded partly by the Kwanjeong Educational Foundation and by the European Communities under the contract of Association between EURATOM and CCFE. The views and opinions expressed herein do not necessarily reflect those of the European Commission. This work was carried out within the framework of the European Fusion Development Agreement.

References

[1] Romanelli F. *et al* 2012 *Proc. 24th IAEA Fusion Energy Conf. (San Diego, CA, 2012)* www.iop.org/Jet/fulltext/EFDP12032.pdf

[2] ITER Physics Basis Expert Group on Disruptions, Plasma Control, and MHD 1999 Chapter 8: Plasma operation and control *Nucl. Fusion* **39** 2577

[3] Tanga A. *et al* 1986 Start-up of the ohmic phase in JET *Tokamak Start-up* vol 26, ed H. Knoepfel (European Physical Society) (New York: Plenum) p 159

[4] Lloyd B., Jackson G.L., Taylor T.S., Lazarus E.A., Luce T.C. and Prater R. 1991 Low voltage ohmic and electron cyclotron heating assisted start-up in DIII-D *Nucl. Fusion* **31** 2031–53

[5] de Vries P.C. *et al* and JET-EFDA Contributors 2013 Characterisation of plasma breakdown at JET with a carbon and ITER-like wall *Nucl. Fusion* **53** 053003

[6] Gribov Y., Humphreys D., Kajiwara K., Lazarus E.A., Lister J.B., Ozeki T., Portone A., Shimada M., Sips A.C.C. and Wesley J.C. 2007 Progress in the ITER Physics Basis: chapter 8. Plasma operation and control *Nucl. Fusion* **47** S385–403

[7] Lloyd B., Carolan P.G. and Warrick C.D. 1996 ECRH-assisted start-up in ITER *Plasma Phys. Control. Fusion* **38** 1627

[8] Stober J. *et al* the ASDEX Upgrade Team and the TJ-II Team, the ITPA integrated Operations Scenarios Group Members, and Experts 2011 ECRH-assisted plasma start-up with toroidally inclined launch: multi-machine comparison and perspectives for ITER *Nucl. Fusion* **51** 083031

[9] Koch R. *et al* and the TEXTOR-94 Team 1999 Low loop voltage start-up of the TEXTOR-94 discharge with ICRF and/or NBI assistance *26th EPS Conf. on Controlled Fusion and Plasma Physics (Maastricht, The Netherlands, 1999)* http://hdl.handle.net/1854/LU-118222

[10] Summers H.P., Dickson W.J., O'Mullane M.G., Badnell N.R., Whiteford A.D., Brooks D.H., Lang J., Loch S.D. and Griffin D.C. 2006 Ionization state, excited populations and emission of impurities in dynamic finite density plasmas: I. The generalized collisional radiative model for light elements *Plasma Phys. Control. Fusion* **48** 263

[11] Kim H.-T., Fundamenski W., Sips A.C.C. and EFDA-JET Contributors 2012 Enhancement of plasma burn-through simulation and validation in JET *Nucl. Fusion* **52** 103016

[12] Philipps V., Mertens Ph., Matthews G.F. and Maier H. 2010 Overview of the JET ITER-like Wall project *Fusion Eng. Des.* **85** 1581–6

[13] Wesson J. 2004 *Tokamaks* (Oxford: Clarendon)

[14] Mech B.V., Haasz A.A. and Davis J.W. 1998 Isotopic effects in hydrocarbon formation due to low-energy H^+/D^+ impact on graphite *J. Nucl. Mater.* **255** 153–64

[15] Davis J.W. and Haasz A.A. 1997 Impurity release from low-z materials under light particle bombardment *J. Nucl. Mater.* **241–3** 37–51

[16] Brezinsek S., Stamp M.F., Krieger K. and JET EFDA contributors 2010 Experience of beryllium sputtering yields on JET *19th Int. Conf. Plamsa Surface Interactions (San Diego, CA, May 2010)* www.iop.org/Jet/fulltext/EFDC100513.pdf

[17] Garcia-Rosales C., Eckstein W. and Roth J. 1994 Revised formulae for sputtering data *J. Nucl. Mater.* **218** 8–17

[18] Kudriavtsev Y., Villegas A., Godines A. and Asomoza R. 2005 Calculation of the surface binding energy for ion sputtered particles *Appl. Surf. Sci.* **239** 273–8

[19] Stangeby P.C. 1999 *The Plasma Boundary of Magnetic Fusion Devices* (Bristol: Institute of Physics Publishing)

[20] Kogut D. *et al* and JET EFDA contributors 2012 Study of JET conditioning with ITER-like wall *38th EPS Conf. on Plasma Physics (Stockholm, Sweden, 2–6 July 2012)* www.iop.org/Jet/fulltext/EFDC120427.pdf

[21] Stamp M.F., Krieger K. and Brezinsek S. 2011 Measurements of beryllium sputtering yields at JET *J. Nucl. Mater.* **415** (Suppl.) S170–3

[22] Philipps V., Loarer T., Esser H.G., Vartanian S., Kruezi U., Brezinsek S. and Matthews G. 2013 Dynamic fuel retention and release under ITER like wall conditions in JET *J. Nucl. Mater.* **438** S1067–71

[23] Roth J., Eckstein W. and Guseva M. 1997 Erosion of Be as plasma-facing material *Fusion Eng. Des.* **37** 465–80

[24] Hirai T. *et al* and JET EFDA 2007 R&D on full tungsten divertor and beryllium wall for JET ITER-like wall project *Fusion Eng. Des.* **82** 1839–45

[25] Lungu C.P., Mustata I., Zaroschi V., Lungu A.M., Anghel A., Chiru P., Rubel M., Coad P., Matthews G.F. and JET-EFDA Contributors 2007 Beryllium coatings on metals for marker tiles at JET: development of process and characterization of layers *Phys. Scr.* **T128** 157–61

[26] Piccolo F., Cenedese A., Ciscato D. and Sartori F. 2003 Non linear model of the gas introduction module for plasma density control at JET *Fusion Eng. Des.* **66–68** 741–7

[27] Coenen J.W. *et al* and JET EFDA contributors 2013 Longterm evolution of the impurity composition and impurity events with the ITER-like wall at JET *Nucl. Fusion* **53** 073043

[28] Kim H.-T., Sips A.C.C., Fundamenski W. and EFDA-JET Contributors 2013 PSI effects on plasma burn-through in JET *J. Nucl. Mater.* **438** S1271–4

[29] Hawryluk R.J. and Schmidt J.A. 1976 Effects of low-z impurities during the start-up phase of a large tokamak *Nucl. Fusion* **16** 775

[30] Belyakov V.A., Vasiliev V.I., Lobanov K.M., Makarova L.P. and Mineev A.B. 2003 Analysis of initial stage of plasma discharge in tokamaks: mathematical model formulation, simulation results, comparison with experiments *PHYCON '03: Proc. 2003 Int. Conf. on Physics and Control (Washington, DC, 2003)* pp 1025–34 doi:10.1109/PHYCON.2003.1237045

[31] Bissell R.C., Johnson P.C. and Stangeby P.C. 1989 A review of models for collisionless one-dimensional plasma flow to a boundary *Phys. Fluids* B **1** 1133

[32] de Vries P.C. *et al* and JET EFDA Contributors 2012 The impact of the ITER-like wall at JET on disruptions *Plasma Phys. Control. Fusion* **54** 124032